the contributions of direct Mn^{2+}–Mn^{2+} and 90° Mn^{2+}–O^{2-}–Mn^{2+} superexchange interactions (Goodenough & Stickler, 1967). The positive region spread between the Mn^{2+} ions suggests a significant contribution of the direct interaction, which is compatible with the antiferromagnetic order observed along the (0001) plane at low temperatures.

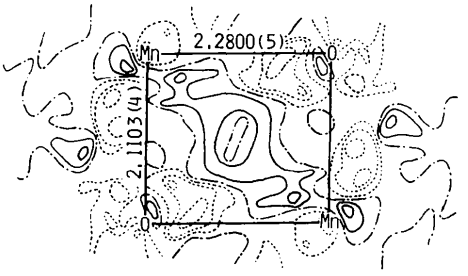

Fig. 4. Section of the difference Fourier map after the final refinement with anharmonic thermal parameters through the plane containing two neighbouring Mn^{2+} ions and the two O^{2-} ions on the shared edge. Contours are at intervals of 0·10 e Å^{-3}. Negative and zero contours are in broken and dashed-dotted lines, respectively. Distances are in Å.

Part of the research cost was met by a Grant-in-Aid for Scientific Research, No. 56420019, from The Ministry of Education, Science and Culture, to which the authors' thanks are due.

References

AKIMITSU, J., ISHIKAWA, Y. & ENDOH, Y. (1970). *Solid State Commun.* **8**, 87–90.
BECKER, P. J. & COPPENS, P. (1974*a*). *Acta Cryst.* A**30**, 129–147.
BECKER, P. J. & COPPENS, P. (1974*b*). *Acta Cryst.* A**30**, 148–153.
BECKER, P. J. & COPPENS, P. (1975). *Acta Cryst.* A**31**, 417–425.
BOND, W. L. (1951). *Rev. Sci. Instrum.* **22**, 344.
GOODENOUGH, J. B. & STICKLER, J. J. (1967). *Phys. Rev.* **164**, 768–778.
International Tables for X-ray Crystallography (1974). Vol. IV. Birmingham: Kynoch Press.
KIDOH, K., TANAKA, K., MARUMO, F. & TAKEI, H. (1984). *Acta Cryst.* B**40**, 92–96.
TAKEI, H., HOSOYA, S. & KOJIMA, H. (1982). *J. Jpn. Assoc. Mineral. Petrol. Econ. Geol.* Special Issue 3, pp. 73–82.
TANAKA, K. & MARUMO, F. (1984). To be published.
TOKONAMI, M. (1965). *Acta Cryst.* **19**, 486.
WILLIS, B. T. M. (1969). *Acta Cryst.* A**25**, 277–300.

Acta Cryst. (1984). B**40**, 332–337

Quantitative Analysis of CBED to Determine Polarity and Ionicity of ZnS-Type Crystals

BY K. ISHIZUKA*

Center for Solid State Science, Arizona State University, Tempe, AZ 85287, *USA*

AND J. TAFTØ†

Department of Physics, Arizona State University, Tempe, AZ 85287, *USA*

(*Received* 15 *October* 1983; *accepted* 23 *February* 1984)

Abstract

The possibility of determining the phase and amplitude of structure factors from convergent-beam electron-diffraction (CBED) patterns, where a few beams are simultaneously at the Bragg position, is studied by quantitative calculations. Dynamical calculations based on a new multislice formula for inclined illumination reproduce well the experimental CBED patterns of GaAs and verify the simple method for determining the absolute polarity of GaAs [Taftø & Spence (1982). *J. Appl. Cryst.* **15**, 60–64]. The calculations demonstrate the effect of the ionicity on the characteristic features of the $\bar{2}00$ disk. A qualitative comparison with experiments shows that the 200 structure factor of GaAs is close to, but slightly smaller than, that obtained from tabulated values for free atoms, suggesting a weak charge transfer from the Ga to the As atoms.

Introduction

Several electron diffraction techniques have been employed to determine structure-factor values. The Bragg reflections as well as the Kikuchi lines contain information about the absolute value of the structure factor and the phase relationship between the structure factors (Kambe, 1957), because many beams are simultaneously excited in most electron diffraction experiments. Two of the techniques, *i.e.* the critical-voltage method (Watanabe, Uyeda & Fukuhara, 1969) and the intersecting Kikuchi-line method (Gjønnes & Høier, 1971), have the advantages that they are essentially insensitive to crystal thickness. The former

* Present address: Institute for Chemical Research, Kyoto University, Uji 611, Japan.
† Present address: Metallurgy and Material Science Division, Brookhaven National Laboratory, Upton, New York 11973, USA.

0108-7681/84/040332-06$01.50

is quite accurate but requires a high-voltage electron microscope with variable voltage, while the latter is less accurate but has more generality. On the other hand, in studies of the intensities in convergent-beam electron diffraction (Goodman & Lehmpfuhl, 1968) or of the thickness oscillation of the direct or a diffracted beam (Ando, Ichimiya & Uyeda, 1974), the crystal thickness has to be known accurately. Thus the convergent-beam electron-diffraction (CBED) method has been mostly restricted to crystals with well defined cleaved planes, and the thickness-oscillation method to wedge crystals.

With the introduction of commercial electron microscopes capable of providing CBED patterns from areas as small as 100 Å in diameter the applicability of CBED has been widely extended, because specimens of sufficiently constant thickness over such small areas can be found in most cases independently of crystal-thinning techniques. It has been demonstrated from simple qualitative arguments that the information about the polarity as well as the structure-factor phase relationships of GaAs can be extracted from one CBED pattern by choosing diffraction conditions similar to those used in the intersecting Kikuchi-line method (Taftø & Spence, 1982). An advantage of CBED, in addition to its high contrast, is the possibility of obtaining information about handedness and polarity, which is lost in the thickness-independent observations.

In this paper we present dynamical calculations of CBED patterns using the multislice method (Cowley & Moodie, 1957; Ishizuka, 1982) to obtain information about the ionicity of GaAs as well as to verify the simple qualitative arguments of Taftø & Spence (1982).

Experimental

Thin crystal areas were obtained by grinding a single crystal of GaAs in an agate mortar. The CBED experiments were performed at 100 kV accelerating voltage using a Philips 400T electron microscope. Fig. 1 shows the GaAs structure as seen along the [011] direction.

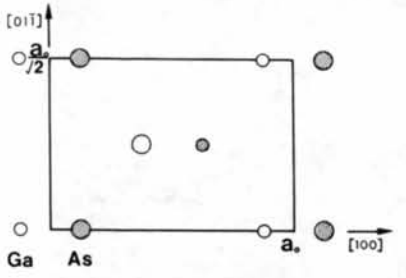

Fig. 1. A schematic drawing of the GaAs crystal structure as seen along the [011] direction. Open and hatched circles show Ga and As atom positions respectively. The atoms located at a basal plane (height 0) are indicated by small circles, and those located midway (height $\frac{1}{2}$) by large circles.

In addition to the mirror symmetry perpendicular to the [01$\bar{1}$] direction, this projection has an approximate mirror plane perpendicular to the [100] direction as far as electron diffraction is concerned, due to the small difference in the Coulomb potential of Ga and As. Thus the exact zone-axis orientation is relatively insensitive to the lack of mirror symmetry perpendicular to the [100] direction. The absence of mirror symmetry is clearly observed by comparing two four-beam CBED patterns tilted away from the [011] zone axis, which are conjugate to each other. The CBED pattern for one such four-beam case is shown in Fig. 2(*a*), where the Bragg condition is fulfilled for the $\bar{2}00$, $\bar{1}\bar{1},1,\bar{1}$ and $91\bar{1}$ reflections. Fig. 2(*b*) shows the conjugate situation where 200, $11,1,\bar{1}$ and $\bar{9}1\bar{1}$ reflections are at the Bragg reflecting positions. Detailed features of the $\bar{2}00$ and 200 diffraction disks for different specimen thicknesses are shown in Fig. 3. The specimen thicknesses were determined by the graphical method (Kelly, Jostons, Blake & Napier, 1975). Notice, particularly for the thinner crystals, that the crossing lines in the disks which are a consequence of scattering *via* the 911 and $11,1,1$-type odd-index reflections appear black in the $\bar{2}00$ disk and white in the 200 disk. This suggests that the interference is destructive between the direct diffraction and the odd-index double diffraction for the $\bar{2}00$ reflection, whereas the interference is constructive for the 200 reflection (Taftø & Spence, 1982).

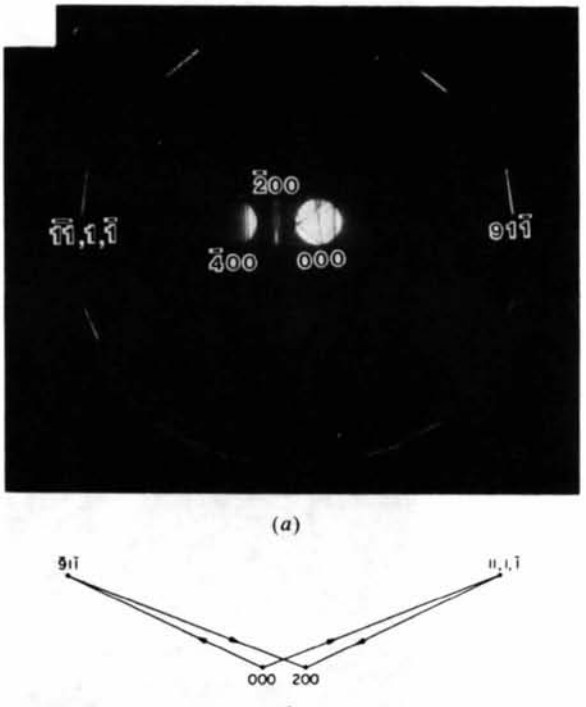

Fig. 2. (*a*) A CBED pattern showing all reflections involved in the $\bar{2}00$ case. (*b*) The two double-scattering paths which contribute to the 200 reflection.

Qualitative interpretation

The dynamical diffraction amplitude for h, k reflection from a parallel-plate crystal can be expressed as follows using the polynomial expression (*e.g.* Cowley, 1981):

$$\Psi(h,k)=\sum_{l}\sum_{n}\sum_{h_1}\cdots\sum_{h_{n-1}}(-i\sigma)^n\Phi(h_1)\cdots$$
$$\Phi(h_{n-1})\Phi(h_n)Z_n(\zeta_1\cdots\zeta_{n-1}\zeta_n). \quad (1)$$

Here h_j's denote three-dimensional indices $h_jk_jl_j$ of each scattering vector and $h=\sum_{j=1}^{n}h_j=(hkl)$. n defines times of interactions. Each Φ represents a kinematical structure factor. ζ_r is an excitation error for rth scattering at h^r, where $h^r=\sum_{j=1}^{r}h_j$. A function Z_n depends on the specimen thickness and on the excitation errors and becomes negligible for large excitation errors. Note the summation over the index l associated with the reciprocal axis normal to the crystal surface. Strictly speaking, a common notation with three indices hkl is not correct to specify the dynamical diffraction amplitude. However, for the reflection hkl near the Ewald sphere, the main contributions to the dynamical diffraction amplitude hk come from the terms where l is equal to the third index of the common notation, since the final excitation error ζ_n is large except for such terms. Thus the common notation with three indices can be used to specify the reflection near the Ewald sphere.

The main contributions to 20 dynamical diffraction (200 reflection) will be a direct scattering: $(000)\rightarrow(200)$ and two double scatterings: $(000)\rightarrow(11,1,\bar{1})\rightarrow(200)$ and $(000)\rightarrow(\bar{9}1\bar{1})\rightarrow(200)$ as indicated in Fig. 2(*b*). At the exact Bragg condition the values of the Z function for these single and double scatterings are proportional to H and $H^2/2$ respectively, where H represents the specimen thickness. Hence 20 and $\bar{2}0$ dynamical diffraction amplitudes (200 and $\bar{2}00$ reflections respectively) can be expressed:

$$\Psi(20)\fallingdotseq-i\sigma H\Phi(200)+(-i\sigma H)^2/2[\Phi(11,1,\bar{1})\Phi(\bar{9}\bar{1}1)+\Phi(\bar{9}1\bar{1})\Phi(11,\bar{1},1)] \quad (2a)$$

and

$$\Psi(\bar{2}0)\fallingdotseq-i\sigma H\Phi(\bar{2}00)+(-i\sigma H)^2/2[\Phi(\overline{11},1,\bar{1})\Phi(9\bar{1}1)+\Phi(91\bar{1})\Phi(\overline{11},\bar{1},1)] \quad (2b)$$

respectively.

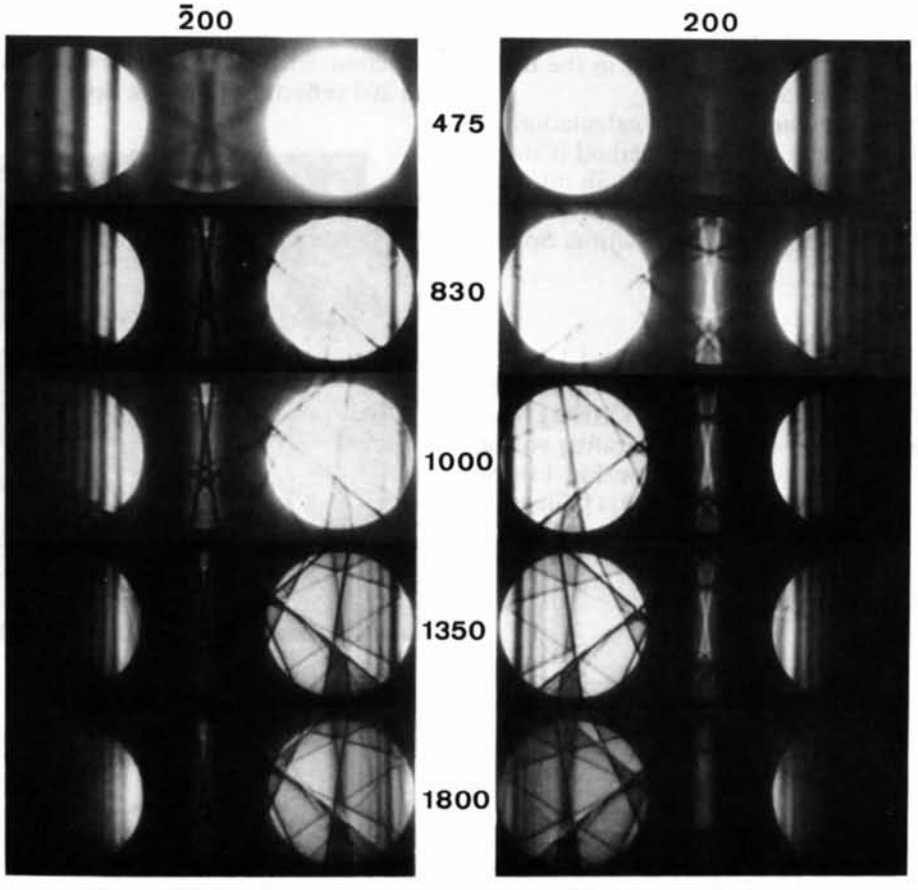

Fig. 3. Detailed features of the 200 (left column) and 200 (right column) diffraction disks for different specimen thicknesses. The estimated specimen thicknesses are indicated in Å.

The kinematical structure factor of GaAs crystal is expressed as

$$\Phi(hkl) = \{f_{Ga}(hkl)\exp[2\pi i(-\tfrac{1}{8})(h+k+l)] + f_{As}(hkl)\exp[2\pi i(+\tfrac{1}{8})(h+k+l)]\}G(hkl) \quad (3)$$

where G is a geometrical factor for a face-centered cubic system, which is four when three indices are all even or odd, otherwise zero. With the Ga and As atoms respectively placed at $(-\frac{1}{8}, -\frac{1}{8}, -\frac{1}{8})$ and $(\frac{1}{8}, \frac{1}{8}, \frac{1}{8})$ as well as equivalent positions, this expression reduces as follows for the participating reflections:

$$\Phi(200) = 8\Delta_{200}i,\ \Phi(\bar{2}00) = -8\Delta_{200}i \quad (4a, b)$$

$$\Phi(91\bar{1}) = \Phi(9\bar{1}1) = 4\sqrt{2}(f_{911} + \Delta_{911}i) \fallingdotseq 4\sqrt{2}f_{911}, \quad (4c)$$

$$\Phi(\bar{9}1\bar{1}) = \Phi(\bar{9}\bar{1}1) = 4\sqrt{2}(f_{911} - \Delta_{911}i) \fallingdotseq 4\sqrt{2}f_{911}, \quad (4d)$$

$$\Phi(11,1,\bar{1}) = \Phi(11,\bar{1},1) = -4\sqrt{2}(f_{11,1,1} - \Delta_{11,1,1}i) \fallingdotseq -4\sqrt{2}f_{11,1,1}, \quad (4e)$$

and

$$\Phi(\bar{1}\bar{1},1,\bar{1}) = \Phi(\bar{1}\bar{1},\bar{1},1) = -4\sqrt{2}(f_{11,1,1} + \Delta_{11,1,1}i) \fallingdotseq -4\sqrt{2}f_{11,1,1}. \quad (4f)$$

Here we rewrite $f_{Ga} = f - \Delta$ and $f_{As} = f + \Delta$, where Δ is positive. Hence the direct scattering into the 200 reflection is almost in phase with the double scattering, while the direct scattering into $\bar{2}00$ is out of phase with the double scattering. This explains the constructive and destructive interferences for the 200 and $\bar{2}00$ reflections, respectively, at relatively thin regions (Taftø & Spence, 1982).

The expressions of the dynamical diffraction amplitudes (2) also illustrate thickness dependence. The single scattering is proportional to specimen thickness, whereas the double scattering is proportional to the square of the thickness. The contribution from the double scattering will become dominant over the single scattering from a certain specimen thickness, and high intensity is expected at the Bragg positions of $\bar{2}00$ as well as 200 reflections. The angular dependence of the diffraction amplitude is interpreted as follows. The double scattering involves the excitation errors at $\bar{9}1\bar{1}$ and $11,1,\bar{1}$ or $91\bar{1}$ and $\bar{1}\bar{1},1,\bar{1}$ for 200 or $\bar{2}00$ cases, respectively. Because the excitation errors for large scattering vectors change rapidly with the incident-beam direction, the contribution from the double scattering is restricted to near the Bragg position. This explains the appearance of two minima surrounding the central maximum in the $\bar{2}00$ reflection disk at thick regions. At these incident-beam directions the reduced contribution from the double-scattering paths cancels the contribution from the single scattering.

Calculations and discussions

A CBED simulation program has been developed for a PDP-11/34 with an AP400 array processor. This program uses a new multislice formula (Ishizuka, 1982) for a large-tilt illumination. Multislice calculations are carried out for each incident-beam direction by changing the propagation function. The effect of reprojection of the potential distribution is found to be negligible. The convolution in the multislice iteration is performed very quickly using a two-dimensional fast Fourier transform routine on the AP400 core memory. The number of beams involved in the calculation is restricted by the AP400 core size, provided that the host computer has sufficient memory.*

The angle between the central direction of the incident beam and the [011] axis is 13·5° for the four-beam situations shown in Fig. 2. The accelerating voltage of 100 kV is assumed and each calculation includes the reflections within a radius of 3 Å^{-1}. The *Pendellösung* plots (thickness dependence) of the scattering amplitudes are shown in Fig. 4. The amplitude of the $\bar{2}00$ reflection is small up to about 1000 Å due to the destructive interference (Fig. 4*a*), whereas

* In our case the number of beams is restricted to 4096 (4K). The core sizes of PDP-11/34 and AP400 are 64K words (16 bits) and 36K words (24 bits) respectively. The maximum core size of AP400 is 64K words.

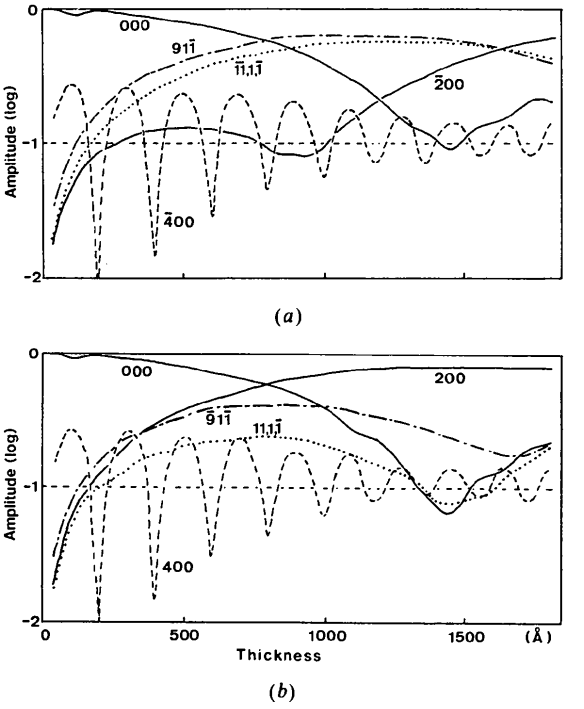

Fig. 4. *Pendellösung* plots of scattering amplitudes for two four-beam conditions. (*a*) and (*b*) show the $\bar{2}00$ and 200 cases respectively.

the amplitude of the 200 reflection increases more rapidly with thickness due to constructive interference (Fig. 4*b*). Another important feature demonstrated in Fig. 4, except for the 400-type reflection, is the long extinction lengths for the reflections involved. Thus the quantitative calculations with many beams have verified the qualitative arguments including only the reflections close to the Ewald sphere to predict the features of the 200 and $\bar{2}00$ reflections and the simple method for determining the absolute polarity of GaAs and other crystals with zinc blende structure (Taftø & Spence, 1982).

Rocking curves (angular dependence) of the scattering intensities across each Bragg position along the [100] axis are shown in Fig. 5, where the specimen thickness is 1400 Å. A small maximum appears at the exact Bragg position for the $\bar{2}00$ reflection. The peak positions of the odd-index reflections slightly shift from the Bragg position. Since the single scattering and the double scattering *via* the $\bar{2}00$ reflection interfere with each other, these peaks should appear at the exact Bragg position when the structure factors of the odd-index reflections have no imaginary component. This is not the case [see (4)], and the contributions from the single and double scatterings are slightly out of phase at the exact Bragg position. This phase difference is compensated by the phase change of the Z function introduced by a small change of the incident-beam direction from the exact Bragg position.

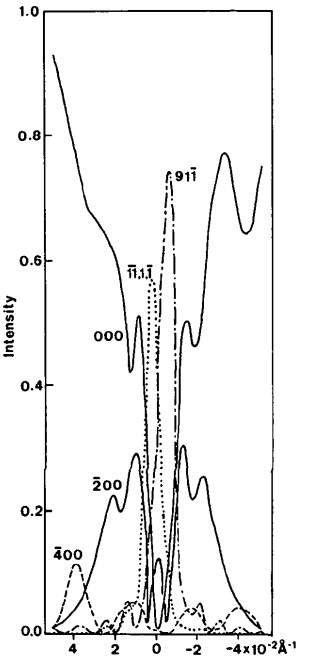

Fig. 5. Rocking curves along the [100] axis for some reflections of the $\bar{2}00$ case at the specimen thickness of 1400 Å. The deviation from each Bragg position is expressed in the reciprocal-space unit ($Å^{-1}$). (The distance between 000 and $\bar{2}00$ reflections is 0·1769 $Å^{-1}$.) Incident beam of unit intensity is assumed.

Rocking curves of the $\bar{2}00$ reflection for different specimen thicknesses are shown in Fig. 6. The intensity at the exact Bragg position increases gradually with thickness. Two minima corresponding to the dark lines in the experimental $\bar{2}00$ diffraction disk are reproduced. The minimum distance between these lines (gap distance) is relatively independent of specimen thickness.

On the other hand, the corresponding gap distances in ZnSe and ZnS are different from that in GaAs (Taftø, 1982): The gap is smallest in ZnS and also the gap in ZnSe in somewhat smaller than that in GaAs. This suggests that the gap distance decreases with increasing magnitude of the 200 structure factor. A similar trend has been observed in studies of $Ga_{1-x}Al_xAs$ with different values of x (Liliental & Ishizuka, 1982).

A question which thus arises is whether the gap distance can be used to determine the value of the 200 structure factor, in other words, the ionicity. Because the 200-type structure factor depends on the difference Δ of the atomic scattering factors of Ga and As, this low-index reflection is very sensitive to charge transfer between these two species, and thus to the ionicity of GaAs. Calculations were carried out varying the 200-type structure factor, and these results are summarized in Fig. 7. The intensity of the central maximum of the $\bar{2}00$ reflection is quite insensitive to the value of the 200 structure factor. This demonstrates that the main contribution comes from the double scattering including the odd-index structure factors. On the other hand, the side maxima (see Fig. 6) increase with increasing 200 structure factor, since their intensity is determined by single scattering. The gap distance, which depends on the balance between the single and double scatterings, varies monotonically with the 200 structure factor. Thus it may be possible to determine the ionicity from the gap distance.

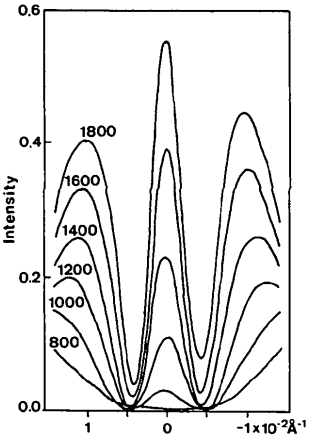

Fig. 6. Rocking curves of the $\bar{2}00$ reflection for different specimen thicknesses. The number on each line shows the specimen thickness in Å.

Another important factor affecting the gap distance is the thermal vibration of atoms to which the high-index structure factors are contrariwise sensitive. The effect of the thermal vibration is also studied by changing the Debye–Waller factor. Fig. 8 summarizes the results, which demonstrate the dependency of the gap distance on the Debye–Waller factor. Since the feature of the $\bar{2}00$ CBED pattern is sensitive to the ionicity of GaAs as well as the Debye–Waller factor, it is difficult to estimate these two parameters independently only from the easily measurable gap distance on the $\bar{2}00$ disk. However, if the value of the Debye–Waller factor is larger than 0·45 Å^2,* then a qualitative comparison with the experimental gap distances shows that the 200 structure factor should be reduced as compared to that obtained from the scattering factors based on the relativistic Hartree–Fock calculations for the free, neutral Ga and As atoms (*International Tables for X-ray Crystallography*, 1974). This suggests a weak charge transfer from the Ga to the As atoms.

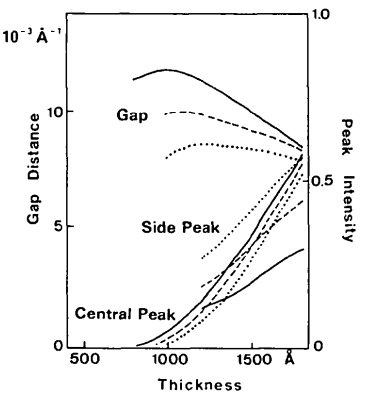

Fig. 7. Effects of the 200-type structure factor on the features of the $\bar{2}00$ CBED pattern. Solid, dashed and dotted lines show the results for the 200 structure factor multiplied by 0·8, 1·0 and 1·2, respectively, where $B = 0{\cdot}45$ Å^2.

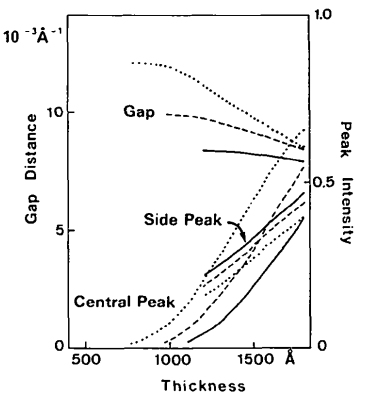

Fig. 8. Influence of the Debye–Waller factor on the $\bar{2}00$ CBED pattern. Solid, dashed and dotted lines show the results for which $B = 0{\cdot}60$, 0·45 and 0·30 Å^2 respectively.

The authors acknowledge the support of the NSF HREM facility in the Center for Solid State Science at Arizona State University (Grant No. CHE7916098) and the NSF Grant No. DMR8002108.

* The value 0·60 Å^2 is tabulated for GaAs in *International Tables for X-ray Crystallography* (1968).

References

ANDO, Y., ICHIMIYA, A. & UYEDA, R. (1974). *Acta Cryst.* A**30**, 600–601.

COWLEY, J. M. (1981). *Diffraction Physics.* Amsterdam: North-Holland.

COWLEY, J. M. & MOODIE, S. F. (1957). *Acta Cryst.* **10**, 609–619.

GJØNNES, J. & HØIER, R. (1971). *Acta Cryst.* A**27**, 313–316.

GOODMAN, P. & LEHMPFUHL, G. (1968). *Acta Cryst.* A**24**, 339–347.

International Tables for X-ray Crystallography (1968). Vol. III, § 3.3. Birmingham: Kynoch Press.

International Tables for X-ray Crystallography (1974). Vol. IV, § 2.4. Birmingham: Kynoch Press.

ISHIZUKA, K. (1982). *Acta Cryst.* A**38**, 773–779.

KAMBE, K. (1957). *J. Phys. Soc. Jpn*, **12**, 13–31.

KELLY, P. M., JOSTSONS, A., BLAKE, R. G. & NAPIER, J. G. (1975). *Phys. Status Solidi A*, **31**, 771–780.

LILIENTAL, Z. & ISHIZUKA, K. (1982). *Proceedings of the 40th Annual Meeting of the Electron Microscopy Society of America, Washington, DC*, pp. 448–449. Baton Rouge: Claitor.

TAFTØ, J. (1982). Unpublished results.

TAFTØ, J. & SPENCE, J. C. H. (1982). *J. Appl. Cryst.* **15**, 60–64.

WATANABE, D., UYEDA, R. & FUKUHARA, A. (1969). *Acta Cryst.* A**25**, 138–140.